Identification of a novel interplay between intestinal bacteria and metabolites in Chinese patients with IgA nephropathy via integrated microbiome and metabolome approaches

Hongwei Wu[1], Donge Tang[2], Fengping Zheng[2], Shanshan Li[2], Xinzhou Zhang[2], Lianghong Yin[1], Fanna Liu[1], Yong Dai[2]

[1]Department of Nephrology and Blood Purification, The First Affiliated Hospital of Jinan University, Jinan University, Guangzhou, China; [2]The First Affiliated Hospital of Southern University of Science and Technology, The Second Clinical Medical College of Jinan University, Shenzhen People's Hospital, Shenzhen, China

Contributions: (I) Conception and design: H Wu, Y Dai, F Liu; (II) administrative support: Y Dai, L Yin; (III) provision of study materials or patients: D Tang, F Zheng, X Zhang; (IV) collection and assembly of data: S Li, F Zheng; (V) data analysis and interpretation: H Wu; (VI) manuscript writing: All authors; (VII) final approval of manuscript: All authors.

Correspondence to: Yong Dai. The First Affiliated Hospital of Southern University of Science and Technology, The Second Clinical Medical College of Jinan University, Shenzhen People's Hospital, Shenzhen, China. Email: daiyong22@aliyun.com. Lianghong Yin; Fanna Liu. The First Affiliated Hospital of Jinan University, Jinan University, Guangzhou, China. Email: yin-yun@126.com; 13560421216@126.com.

Background: Immunoglobulin A nephropathy (IgAN) is the most common form of primary glomerulonephritis. The intestinal microbial ecosystem and metabolic network of IgAN have not been systematically analyzed. The present study aims to improve understanding of the gut microbiota and its metabolic capabilities to facilitate the development of diagnostic, therapeutic, and prognostic methods for IgAN.

Methods: We characterized the gut microbiota and metabolic patterns of fecal and serum samples of IgAN patients and healthy controls from the south of China using 16s ribosomal RNA gene sequencing and liquid chromatography-tandem mass spectrometry, respectively, and bioinformatics approaches.

Results: We found that the relative abundances of *Streptococcus* and *Enterococcus* were higher in IgAN patients, whereas *Bacteroidetes* and *Bacteroides* were lower. Changes in the gut microbiota of IgAN affected the metabolism and absorbance of microbiota-associated metabolites, in particular polyunsaturated fatty acids, free amino acid, and oligopeptides, and activated the phenylalanine metabolism pathway, thereby constructing a unique metabolic system of IgAN. We identified six pivotal metabolites, including bilirubin, trimethoprim, stearamide, phenylalanine, cis-9,10-epoxystearic acid, and phosphatidylethanolamine 17:0, that connected the metabolic networks of the gut and blood. Additionally, 5-hydroxyeicosatetraenoic acid and 5-hydroxy-6E,8Z,11Z-eicosatrienoic acid were shown to be associated with the classification of glomerular sclerosis.

Conclusions: We establish a relational network between microbiota, fecal metabolites, and serum metabolites in IgAN. The core microbiota and metabolites identified have promising value in therapeutic applications.

Keywords: Immunoglobulin A nephropathy (IgAN); microbiome; metabolome; metabolic network

Submitted Mar 14, 2020. Accepted for publication Sep 30, 2020.
doi: 10.21037/atm-20-2506
View this article at: http://dx.doi.org/10.21037/atm-20-2506

Introduction

Immunoglobulin A nephropathy (IgAN), the most common form of primary glomerulonephritis (PGN) worldwide, is particularly prevalent in Asia and accounts for almost 45% of all PGN cases in China (1,2). The etiology and pathogenesis of primary IgAN are complicated and not entirely clear, but are thought to involve abnormally glycosylated IgA1 deposition, which contributes to local inflammation, mesangial proliferation, and glomerular fibrosis (3-6). Changes in components of the mucosal environment, such as exogenous oral and intestinal antigens, have a potential impact on the occurrence and progression of IgAN by regulating the synthesis of IgA, as IgA is known to be produced mainly by the mucosal immune system (7,8).

With the development of 16S ribosomal RNA (rRNA) sequencing analysis, emerging evidence has linked the microbiome to IgAN (7,9). It was speculated that a shift in gut microbiota stimulated epithelial cells to secrete excessive B-cell activating factor (BAFF) and a proliferation-inducing ligand (APRIL), which induced the overproduction of IgA and maintained tolerogenic immune responses (10). Additionally, microbial metabolites could be used to represent the function of microbial activities and act as intermediate phenotypes between the host and microbiota (11). For instance, indoxyl sulfate, p-cresyl sulfate, and trimethylamine-N-oxide are intestinal metabolites closely related to the progression of chronic kidney disease (CKD) (12). Enterotoxin-activated immune cells in the intestinal mucosa continue to produce inflammatory cytokines, leading to chronic systemic inflammatory responses (13).

The relational network among microbiota, fecal metabolites, and serum metabolites has not been systematically analyzed. Knowledge of the gut microbiota and metabolites of IgAN patients should contribute to the identification of potential biomarkers that correlate with clinical symptoms. Therefore, the present study aimed to identify a particular network between gut bacteria and metabolites in IgAN and to explore the influence of metabolites on clinical symptoms for application in clinical practice.

Methods

Study design

Forty-five participants, including 15 IgAN patients aged 22–56 years and 30 age-matched healthy controls (HCs) were enrolled in the present study. All participants were recruited from Shenzhen People's Hospital. IgAN patients were diagnosed by postoperative pathological examinations, and patients with diabetes mellitus, recent infection, severe liver disease, malignancies, cardiac insufficiency, autoimmune diseases, secondary IgAN, or alcohol abuse were excluded. Participants recruited for the present study were treatment-naïve IgAN patients who had not taken any drugs (e.g., antibiotics or aspirin) or nutritional supplements for at least two months. All subjects were Han Chinese from southern China with comparable eating habits and lifestyles. The present study was conducted following the principles of the Declaration of Helsinki (as revised in 2013) and was authorized by the ethics board of Shenzhen People's Hospital (LL-KY-2019514). All participating individuals provided signed informed consent. Clinical data (age, sex, body mass index, and hypertension), biochemical indices, and the Oxford classification of IgAN were recorded. The estimated glomerular filtration rate (eGFR) was assessed using CKD epidemiology (14,15).

Metabolite extraction from fecal and serum samples

Fecal and serum samples were collected after overnight fasting. After adding 1,000 μL extract solvent (2:2:1 acetonitrile-methanol-water containing 1 μg/mL internal standard), fecal samples were vortexed for 30 seconds, homogenized at 45 Hz for 4 minutes, and sonicated for 5 minutes in an ice-water bath. 300 μL of methanol containing 1 μg/mL internal standard was added to the serum samples, vortexed for 30 seconds, and sonicated for 10 minutes in an ice-water bath. The samples were then incubated at –20 ℃ for 1 hour and centrifuged at 12,000 rpm at 4 ℃ for 15 minutes. A quality control sample was acquired by mixing an equal amount of supernatant from each of the samples.

DNA extraction and 16S rRNA gene sequencing

A PowerSoil DNA Isolation Kit (Qiagen, Germany) was used to extract genomic DNA from feces. DNA size and integrity were verified using 1% agarose gel electrophoresis. NanoDrop spectrophotometry (NanoDrop) was used to determine DNA concentrations. Primers (319F: 5'-ACTCCTACGGGAGGCAGCAG-3'; 806R: 5'-GGACTACHVGGGTWTCTAAT-3') targeting the V3 and V4 hypervariable regions of the 16S rRNA gene were used for 16s rRNA-based amplification. After amplification, polymerase chain reaction products were mixed with

AMPure XP beads (Beckman Coulter, UK) at a ratio of 1:1.5, and the fragments were screened and cleaned. After purification and library construction, the amplicons were quantified using a Qubit fluorometer (Invitrogen, USA) and sequenced on a HiSeq PE250 sequencing instrument (Illumina, USA).

16s rRNA data analysis

Paired-end reads were produced and allocated to each sample according to the marked barcodes. Reads were further merged using FLASH software version 1.2.11 (16). After high-quality filtering of the raw tags using Trimmomatic software version 0.33 (17), we used UCHIME software version 8.1 (18) to remove chimeric sequences and acquire high-quality clean tags. Sequences with >97% similarity were allocated to the same operational taxonomic unit (OTU) using USEARCH software version 10.0 (19). RDP Classifier version 2.2 was applied to annotate species based on the 16S SILVA online database release 128 (20,21). We used PyNAST (http://biocore.github.io/pynast/) to analyze phylogenetic differences in dominant OTUs (22). Alpha diversity analysis was performed using Mothur version v.1.30 (http://www.mothur.org/) (23). We used unweighted principal coordinate analysis (PCoA) to calculate beta diversity. Linear discriminant analysis (LDA) of effect size (http://huttenhower.sph.harvard.edu/lefse/) was used to compare species between groups, and LDA was used to estimate the influence of abundance of each species. Metastats analysis (http://metastats.cbcb.umd.edu/), an improved statistical method for the analysis of metagenomic data, was used to screen significant species.

Liquid chromatography-tandem mass spectrometry data acquisition

Liquid chromatography-tandem mass spectrometry (LC-MS/MS) analysis was carried out using a UHPLC system (Agilent Technologies, USA). The liquid included 2 phases: mobile phase A (5 mmol/L ammonium acetate in water as the negative, and 0.1% formic acid in water as the positive) and mobile phase B (acetonitrile). The gradient program was as follows: 0 minutes, 1% B; 1 minute, 1% B; 8 minutes, 99% B; 10 minutes, 99% B; 10.1 minutes, 1% B; and 12 minutes, 1% B. A total of 2 μL of each sample was injected at a flow rate of 0.5 ml/minutes. A Q Exactive (QE) mass spectrometer was used to acquire MS/MS spectra. Operation of the electrospray ionization (ESI) source used the following parameters: sheath gas flow rate =45 arb, aux gas flow rate =15 arb, full MS resolution =70,000, capillary temperature =400 ℃, collision energy =20/40/60 eV in a normalized collision energy model, MS/MS resolution =17,500, and spray voltage =4.0 kV (positive)/–3.6 kV (negative). ProteoWizard was used to convert the LC-MS/MS data to mzXML format, and the raw data were processed, cleaned, and aligned using MAPS software version 1.0 (24). Finally, we used the MS2 database for further analysis of metabolites.

LC-MS/MS-based metabolomics data analysis

The ionization source of the QE platform was ESI in the positive ion mode and negative ion modes. After relative standard deviation de-noising and standard internal normalization, the final dataset was imported to the SIMCA software package version 15.0.2 for further analysis (25). To visualize group separation and to highlight phenotypic differences between the groups, supervised orthogonal projections to latent structures-discriminant analysis (OPLS-DA) was performed based on principal component analysis (PCA) (26). The quality of the model was verified using 7-fold cross-validation. The validity of the model was evaluated using R^2 (model's interpretability to variables) and Q^2 (predictability of the model) values obtained from 7-fold cross-validation. The variable importance in the projection (VIP) of the first principal component of the OPLS-DA analysis was determined to identify differential metabolites. Kyoto Encyclopedia of Genes and Genomes (http://www.genome.jp/kegg/) and MetaboAnalyst (http://www.metaboanalyst.ca/) were used for pathway-enrichment analyses.

Statistical analyses

Differential analysis was performed using 2-tailed Student's *t*-tests for measurement data or χ^2-tests for enumeration data. Pearson's correlation analysis was used to assess correlations between gut bacteria and metabolites. Metabolites with $P<0.05$ and VIP >1 were considered significantly changed metabolites. All data were analyzed with GraphPad Prism 7.0 software. Heat maps were created using R version 3.5.3 (https://www.r-project.org/), and Cytoscape version 3.7.1 (https://cytoscape.org/) was used to construct the relational network.

Results

Summary of clinical characteristics

All patients were diagnosed with IgAN by pathological examination. General condition surveys (e.g., age, body mass index, and blood pressure) of the two groups showed no statistically significant differences (P>0.05). However, there were significant differences in 24 hours proteinuria, serum albumin, creatinine, and uric acid between the HC and IgAN groups (P<0.05) (Table S1). Information on the histological grades of IgAN patients is shown in Table S2.

Bacterial OTUs and diversity analyses

Total intestinal bacteria from 15 IgAN patients and 30 HCs were analyzed by 16S rRNA gene sequencing. After quality control, pyrosequencing analysis yielded an average of 58,188 effective tags (average length: 414 bp) per sample. Sequences with >97% similarity were classified into the same OTU. A total of 408 and 403 OTUs were identified in the HC and IgAN groups, respectively, including 395 shared OTUs (*Figure 1A*). Based on the OTUs, paired *t*-tests showed significant differences in bacterial diversity (Simpson and Shannon diversity indices), but not species abundance (Chao1 and abundance-based coverage estimator) between the HC and IgAN groups (*Figure 1B*). Rarefaction curves suggested that sequencing depth and coverage were sufficient (*Figure 1C*). PCoA plots were applied to evaluate similarities between microbial communities from each HC and IgAN patient and the result revealed an obvious variation between the two groups (*Figure 1D*).

Abundance distribution and differential analysis of different biologic classifications

Ten main bacterial phyla were identified (*Figure 1E*). *Actinobacteria*, *Bacteroidetes*, *Firmicutes*, *and Proteobacteria* represented more than 97% of all 16S rRNA sequences in the two groups. The relative abundance of *Proteobacteria* was higher in IgAN patients (median value: 15%) than HCs (median value: 7.97%). The opposite trend was found for *Bacteroidetes*, which was lower in IgAN patients (9.81%) than in HCs (23.2%) (*Figure 1F*). The relative abundance of OTUs was assessed at the class, order, family, genus, and species levels, and the top 10 microbiota are shown in Figure S1. At the genus level, *Blautia* (HCs: 4.56%, IgAN patients: 10.2%) showed a remarkable upward trend in the IgAN group, whereas *Bacteroides* (HCs: 15.3%, IgAN patients: 9.5%) and *Faecalibacterium* (HCs: 15.3%, IgAN patients: 9.5%) showed a downward trend in the IgAN group. Furthermore, *Streptococcus* (HCs: 0.77%, IgAN patients: 5.75%) and *Enterococcus* (HCs: 0.1%, IgAN patients: 6.7%) were nearly absent among HCs, but were highly abundant among IgAN patients (*Figure 1G*).

We compared taxa using Metastats analysis with a *P*-value cutoff <0.05 and an LDA cutoff >4 (*Figure 2A*) to predict the core microbiota for each bacterial classification (*Table 1*). Cladograms based on LDA >4 show the evolutionary relationship between each microbe (*Figure 2B*). The results showed that the phylum *Bacteroidetes*, the family *Bacteroidaceae*, and the genus *Bacteroides* were more abundant in the HC group and might be the principal taxa among healthy individuals. At the genus level, we found that *Streptococcus* and *Enterococcus* were more abundant in IgAN patients than HCs. Interestingly, *Streptococcus* and *Enterococcus* accounted for a low proportion of the microbes in HCs, but were highly abundant in the fecal samples of IgAN patients, indicating that the two microbes could be significant features of IgAN.

Identification of metabolites in fecal and serum samples

OPLS-DA models demonstrated that the metabolic profile of the IgAN group was significantly different from that of the HC group (Figure S2). Based on the screening criteria, VIP >1 and P<0.05, 131 and 80 differential metabolites were found in fecal and serum samples, respectively (Tables S3,S4). Lipids and lipid-like molecules (e.g., long-chain fatty acids and phospholipids), alkaloids, and fatty acid amides showed a downward trend in the fecal metabolites of IgAN patients, whereas free amino acids, oligopeptides, and carboxylic acids showed an upward trend. A decrease in lipids (medium-/long-chain fatty acids) and an increase in free amino acids and polypeptides were also observed in serum samples (*Figure 3A*). To identify core fecal metabolites, we determined the top 10 differential metabolites based on the criteria VIP >2 and log fold change >4 (*Figure 3B*). Notably, 6 metabolites–bilirubin, trimethoprim, stearamide, phenylalanine, cis-9,10-epoxystearic acid, and phosphatidylethanolamine (PE lyso 17:0)—were found in both fecal and serum samples, and could potentially serve as core metabolites for IgAN (*Figure 3C*). The top 10 serum metabolites and the expression levels of the 6 core metabolites in the serum samples are shown in *Figure 3D* and *E*. Furthermore, 2 pathways of metabolites from the fecal samples of IgAN

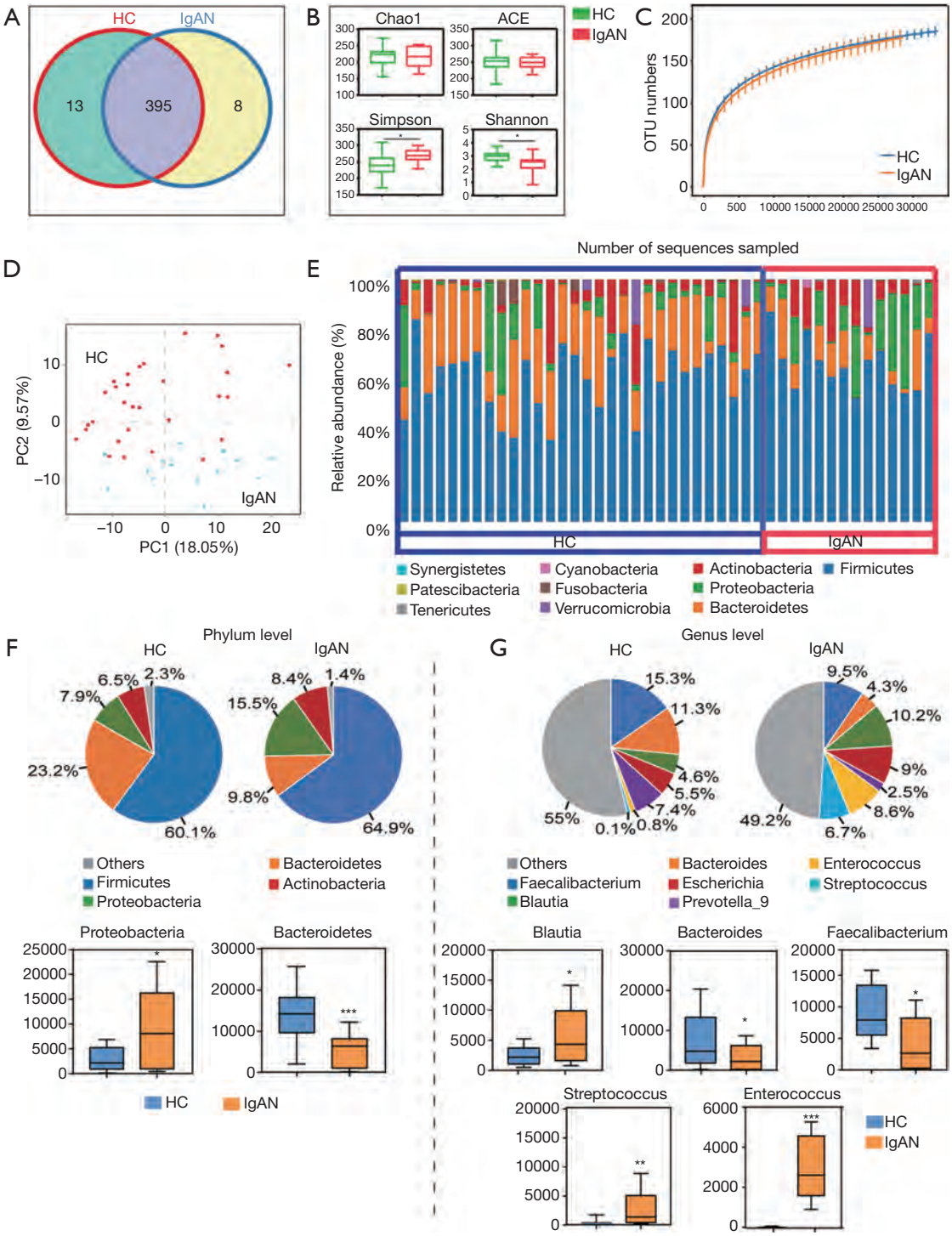

Figure 1 Microbiota diversity analysis. Operational taxonomic units (OTUs) of immunoglobulin A nephropathy (IgAN) and healthy control (HC) groups. (B) Richness estimator (Chao1), abundance-based coverage estimator (ACE), and diversity indices (Simpson and Shannon) of microbiota from the fecal samples of IgAN and HC groups. (C) Rarefaction curves of microbiota from fecal samples. Means ±95% confidence intervals are shown. (D) Community clustering using principal coordinate analysis of the unweighted UniFrac distance matrix. Change in the relative abundance of bacteria in fecal samples from IgAN and HC groups at the phylum level (E,F) and genus level (G). *, P<0.05; **, P<0.01; ***, P<0.001

Figure 2 Linear discriminant analysis (LDA) is integrated with effect size. (A) Differences in the relative abundance of bacteria in healthy control (HC) and immunoglobulin A nephropathy (IgAN) groups. (B) Cladogram of the phylogenetic distribution of microbes. Each circle represents a classification level from phylum to species from the inner to outer circles. The size of each circle is proportional to relative abundance. Microbes with no significant difference in abundance are shown in green. Microbes with an LDA value >4 in IgAN and HC groups are marked with orange and blue, respectively.

Table 1 Metastats and LEfSe analyses of differential microbes at different levels of biological classification

Bacteria	Metastats analysis			LEfSe analysis	
	HC (mean)	IgAN (mean)	*t*-test	HC (LDA value)	IgAN (LDA value)
Phylum					
Firmicutes	60.1%	64.9%	0.210		<2
Bacteroidetes	23.20%	9.81%	<0.01	4.98	–
Proteobacteria	7.97%	15.00%	0.045	–	<2
Class					
Clostridia	51.8%	47.4%	0.425	<2	
Bacteroidia	23.20%	9.81%	0.001	4.98	–
Bacilli	1.4%	11.6%	0.054		4.65
Order					
Clostridiales	51.8%	47.4%	0.425	<2	
Bacteroidiales	23.20%	9.81%	0.001	4.98	–
Lactobacillales	1.39%	11.6%	0.052		4.64
Family					
Bacteroidaceae	11.30%	4.48%	0.018	4.532	–
Enterococcaceae	0.03%	5.08%	0.009	–	4.48
Streptococcaceae	0.78%	5.76%	0.021	–	4.415
Genus					
Faecalibacterium	15.3%	9.5%	0.048	<2	
Streptococcus	0.77%	8.6%	<0.01	–	4.415
Blautia	4.56%	10.20%	0.030	–	<2
Bacteroides	11.30%	4.30%	0.020	4.61	–
Enterococcus	0.10%	6.70%	<0.001	–	4.48

HC, healthy control; IgAN, immunoglobulin A nephropathy; LDA, linear discriminant analysis; LEfSe, linear discriminant analysis of effect size; Note: Microbes with LDA values >2 and *t*-test P values <0.05 were considered statistically significantly different.

patients, including the arachidonic acid metabolism pathway (impact value: 0.32) and the phenylalanine metabolism pathway (impact value: 0.16), were found to be statistically significant (P<0.05, impact value: >0.1) (*Figure 3F*). The phenylalanine metabolism pathway (impact value =0.12) was also enriched in the serum samples of IgAN patients (*Figure 3G*).

Cross-talk among fecal metabolites, serum metabolites, and intestinal microbes

We performed Pearson correlation analysis to reveal the relationship between fecal bacteria and the essential metabolites identified. We found that *Streptococcaceae* was positively correlated with fecal and serum bilirubin, whereas *Bacteroidetes* was correlated with fecal and serum PE lyso 17:0 (*Figure 4*, Table S5). Significantly, the fecal metabolites bilirubin, phenylalanine, and PE lyso 17:0 were positively correlated with the serum metabolites bilirubin, phenylalanine, and PE lyso 17:0 (r>0.5, P<0.05), respectively, suggesting that these core metabolites might be significant mediators between the intestinal tract and blood circulation (*Figure 4* and Figures S3,S4). Details of the microbe-metabolite network are shown in *Figure 4*.

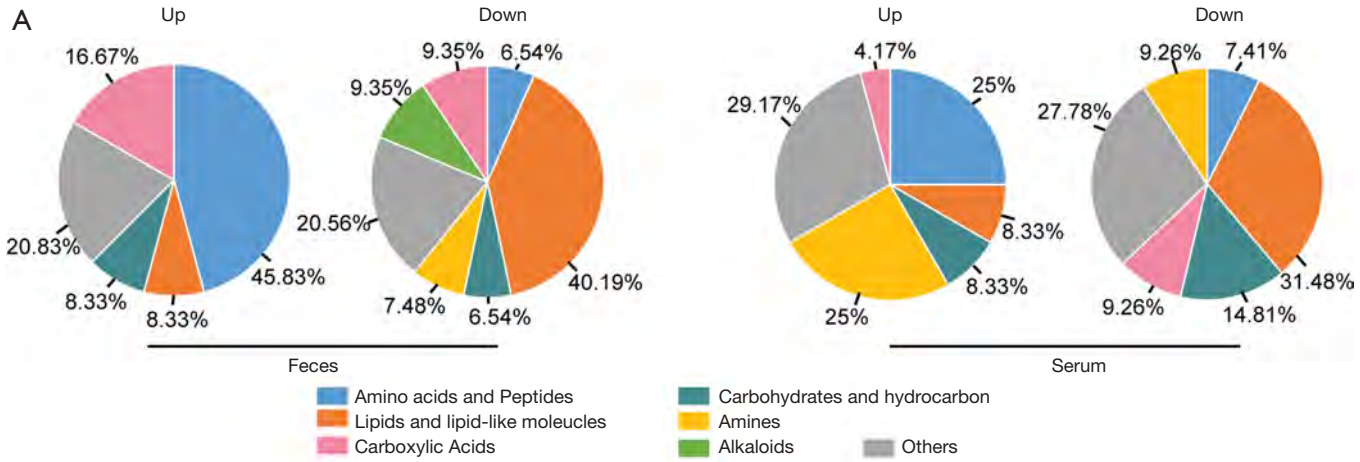

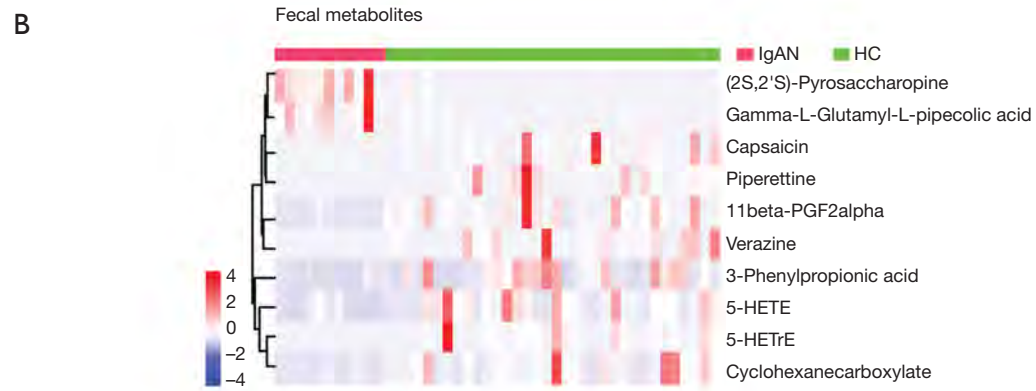

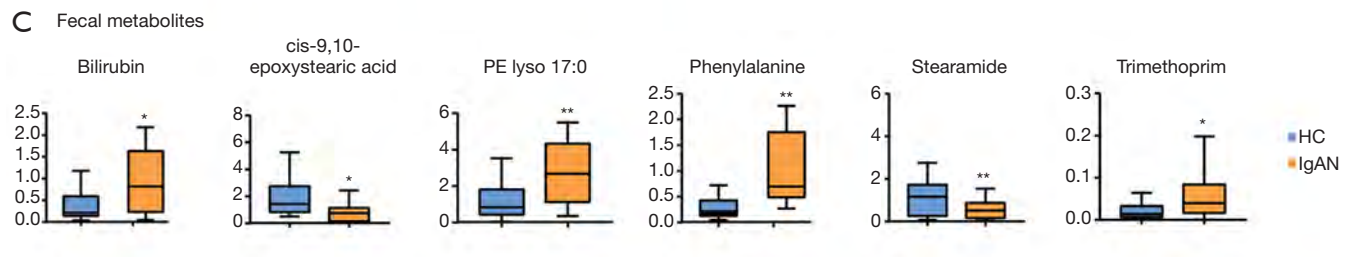

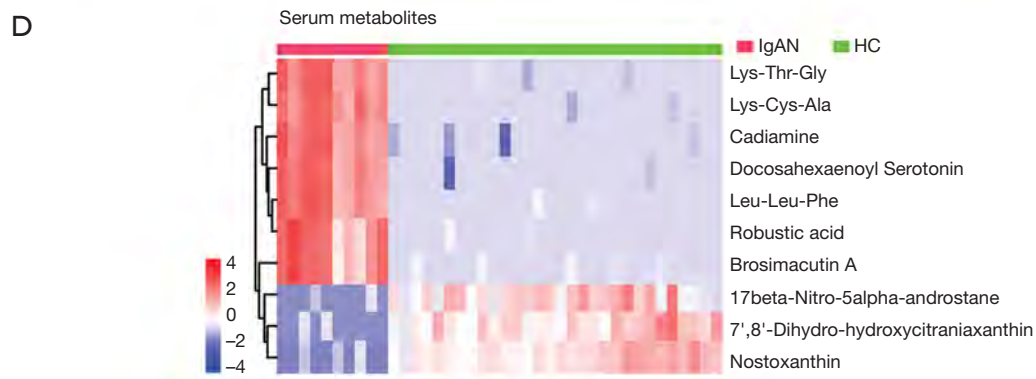

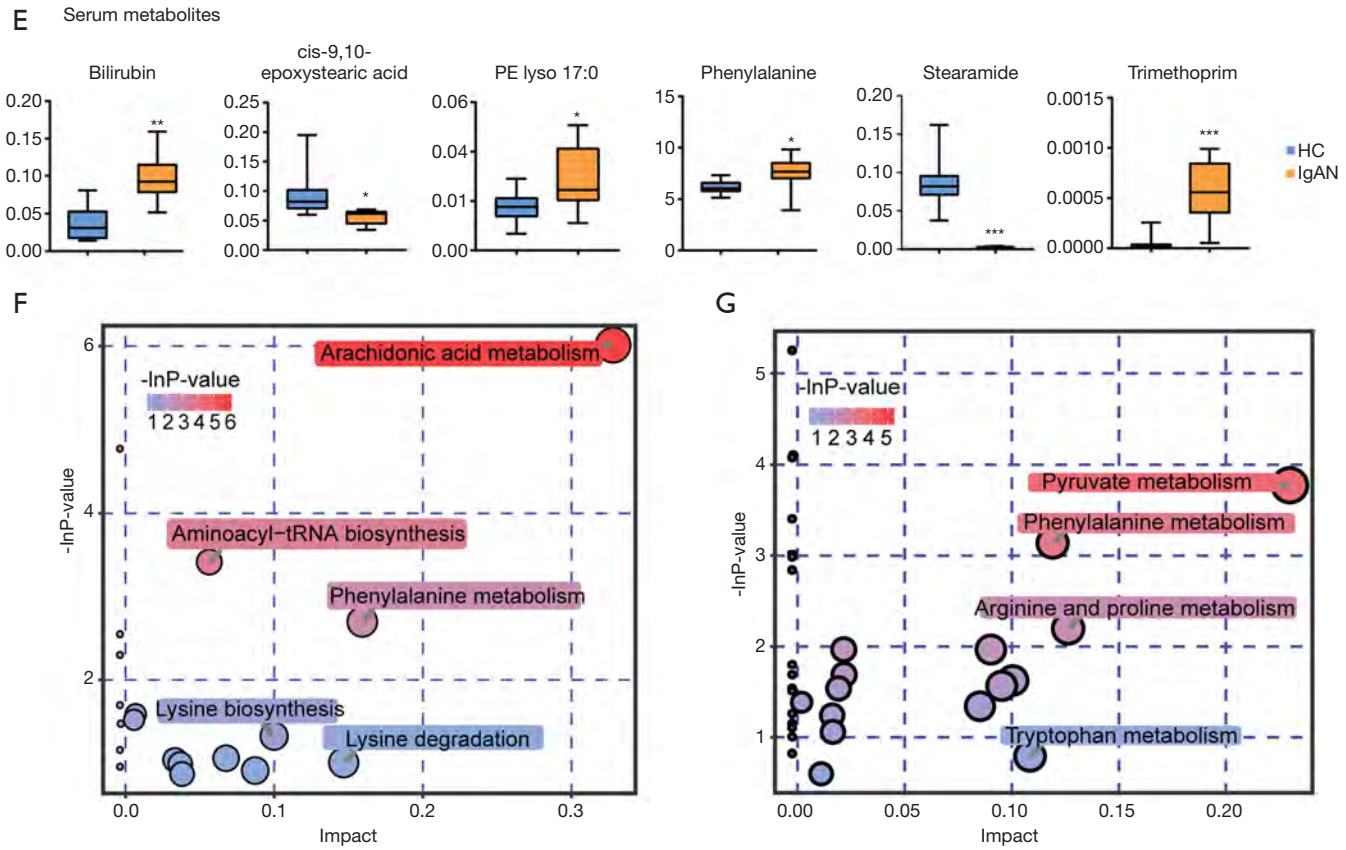

Figure 3 Differential metabolite identification and pathway-enrichment analyses. (A) Altered metabolite class composition for feces and serum. (B) Differential metabolites with variable importance in the projection (VIP) >2 and log fold change >4. Expression of the 6 core metabolites in fecal samples (C) and serum samples (D,E). Metabolic pathway enrichment of fecal samples (F) and serum samples (G). *, P<0.05; **, P<0.01; ***, P<0.001.

Correlation analysis between metabolites and clinical symptoms

We performed *t*-tests to analyze the relationship between the core metabolites identified above and 24-hour proteinuria, eGFR, and pathological classification of IgAN. The results showed that the metabolites were not correlated with 24-hours proteinuria or eGFR. Using the Oxford classification of IgAN, we found that patients with mesangial hypercellularity had higher serum brosimacutin A and robustic acid levels (P<0.05). Also, levels of fecal metabolites 5-hydroxy-6E,8Z,11Z-eicosatrienoic acid (5-HETrE), and 5-hydroxyeicosatetraenoic acid (5-HETE) were lower in patients with severe segmental glomerulosclerosis (*Figure 5A*, Tables S6,S7). No significant correlation was found between the Oxford classification of IgAN and core gut microbes *Streptococcus*, *Bacteroides*, and *Enterococcus* (*Figure 5B*).

Discussion

It is estimated that approximately 100 trillion microorganisms inhabit the human gut, and the total number of microbial genes is approximately 100 times that of the human genome (27). In addition to participating in the metabolism of nutrients and the synthesis of some vitamins, the intestinal microbial ecosystem helps maintain intestinal homeostasis and induces immune system maturation, as well as immune tolerance (28). Additionally, changes in the composition, abundance, and functional genetics of human micro-ecology are closely related to human health and disease (29). Therefore, the gut microbiota and its metabolites may provide feasible early detection tools for IgAN.

Unlike the results of De Angelis, which showed lower microbial diversity in IgAN patients compared with HCs (9), our study indicated that microbial diversity did not differ

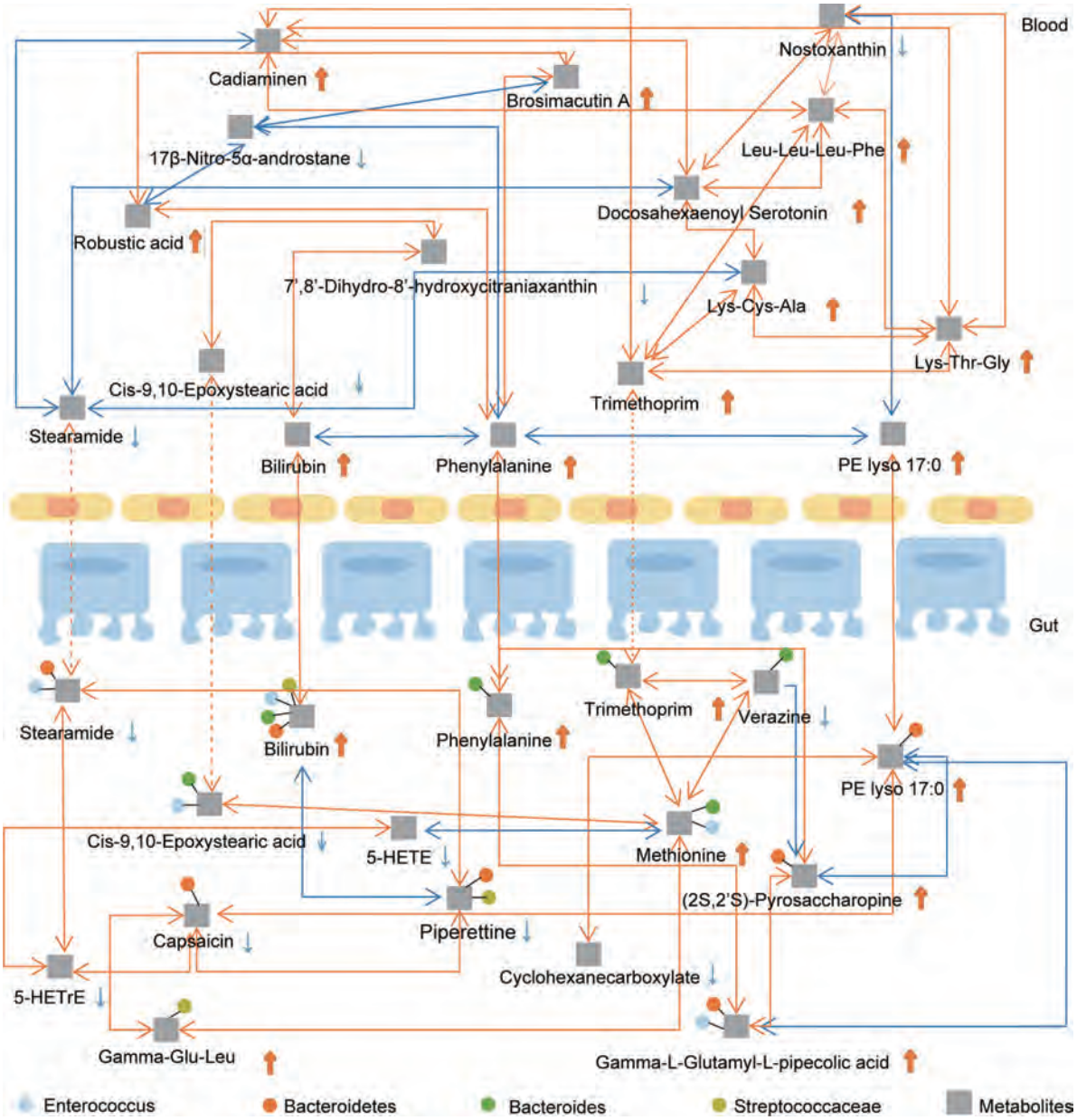

Figure 4 Metabolite network between gut and blood systems in immunoglobulin A nephropathy patients. Blue lines represent negative correlations (r<–0.5), and red lines represent positive correlations (r>0.5). Dotted lines represent |r|<0.5 with no significant correlation. r, Pearson correlation coefficient.

significantly between the two groups based on alpha and beta diversity analyses. However, the relative abundance of some specific bacteria was found to be significantly different. We suspect that the number of certain bacteria, rather than bacterial categories, changes during the early stages of IgAN. It is now known that approximately 1,000 different species inhabit the adult human gut, and the most abundant microbial phyla are *Firmicutes*, *Bacteroidetes*, *Actinobacteria*, and *Proteobacteria* (30,31). This is consistent with the results of our study, in which these microbial phyla accounted for >97% of all species in both the HC and IgAN groups. More importantly, at the genus level, a 2.6-fold decrease in *Bacteroides*, a 7.5-fold increase in *Streptococcus*, and a 67-fold increase in *Enterococcus* were observed in IgAN

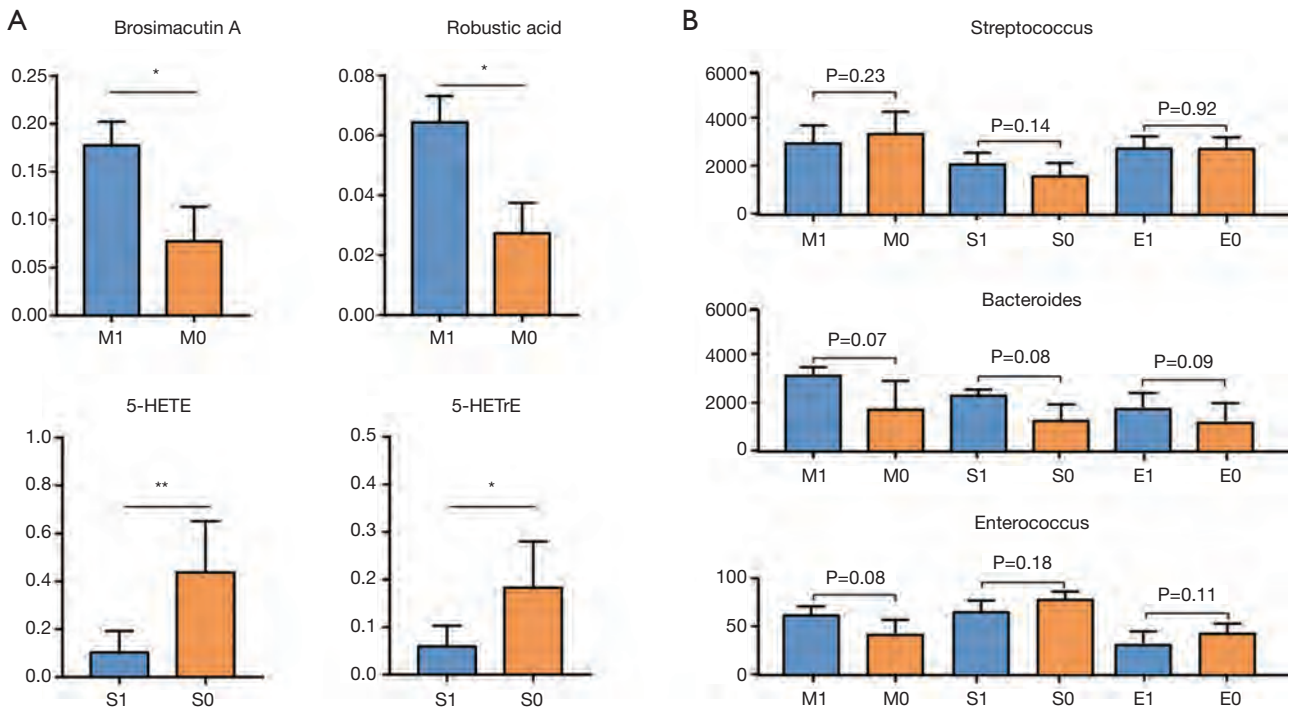

Figure 5 Correlation between the Oxford classification of immunoglobulin A nephropathy (IgAN) and core metabolites and gut microbiota. (A) Significant metabolites associated with Oxford classification. (B) The relative abundance of core intestinal flora in patients with different Oxford classification. M, mesangial hypercellularity; S, segmental sclerosis. *, P<0.05; **, P<0.01.

patients compared with HCs, indicating that a dramatic shift occurred in the fecal microbiome of IgAN patients. A previous study using both 16S DNA and 16S rRNA analyses revealed that *Bacteroides* was less abundant in IgAN patients, although these results were not supported by fecal bacterial culture (9). Our results also showed that the relative abundance of fecal *Streptococcus* was low in HCs, but was significantly increased in IgAN patients. Although a previous study showed no statistical difference in the number of cultivable *Streptococcus* between IgAN and HC groups (9), tissue deposits of IgA-binding streptococcal M proteins are considered an indicator of IgAN pathogenesis (32). Overall, we found that the abundance of Gram-positive bacteria showed an upward trend, whereas Gram-negative bacteria declined. Therefore, we conclude that the effects of the microbiome on IgAN are likely to be associated with holistic dysbiosis rather than specific bacterial species.

As mediators of the functional activity of bacteria, gut microbiota-generated metabolites play an essential role in the development and progression of kidney disease (33,34). In the present study, we identified a greater number of decreasing metabolites (medium-/long-chain fatty acids) and increasing metabolites (amino acids and oligopeptides) in both the fecal and serum samples of IgAN patients. A previous study also reported that some free amino acids (Met, Phe, and Gly) showed an upward trend in the serum or fecal samples of IgAN patients (9), which corresponds to the findings of our study and demonstrates the underlying role of the transformation of amino acids early in the pathogenesis of related diseases. Additionally, an increase in oligopeptides rather than polypeptides was found in our study, suggesting a possible effect of bacterial proteolytic fermentation. Furthermore, impaired protein assimilation has been reported in CKD patients (35), leading to easier absorption of amino acids and oligopeptides due to low energy consumption and non-competitive transport. We also detected a decrease in some fatty acids in IgAN patients, in particular, polyunsaturated fatty acids (e.g., 5-HETE and 5-HETrE). Studies have reported that polyunsaturated fatty acid supplementation can attenuate inflammation, oxidative stress, and tubulointerstitial fibrosis in the remnant kidney (36). Decreasing polyunsaturated fatty acids have not been reported to influence IgAN. It has also been speculated that a reduction in short-chain

fatty acids contributes to the progression of CKD (37). Our results suggest that IgAN is characterized by a decrease in medium-chain fatty acids in fecal samples and long-chain fatty acids in serum samples, but not short-chain fatty acids. In general, we found differential metabolic features in the fecal and serum samples from IgAN patients and HCs.

The species richness of the microbial flora is closely related to metabolic diversity in feces (38). We found that changes in fecal metabolites were caused by a variety of bacteria rather than by a specific gut bacteria (*Figure 4*). Fecal metabolites further affect serum metabolites and lead to changes in body metabolism. for example, the increasing fecal metabolites phenylalanine and bilirubin are proportional to serum phenylalanine and bilirubin levels, respectively. KEGG analysis revealed that the phenylalanine metabolism pathway was enriched in both the fecal and serum samples of IgAN patients. Notably, gut microbiota can produce indoxyl sulfate, a toxin that causes damage to the kidney, by metabolizing phenylalanine (39). In the present study, no correlation was found between metabolites and the clinical measures 24-hours proteinuria or eGFR (7). We found that 5-HETE and 5-HETrE were associated with the classification of segmental sclerosis, indicating that polyunsaturated fatty acids might play a positive role in the kidney (36). To the best of our knowledge, the present study is the first to report an association between metabolites and renal function, and this relationship requires further investigation with larger sample sizes.

At present, systemic corticosteroids and immunosuppressive drugs are the main treatments for IgAN. However, the side-effects of these drugs and high recurrence rates should be taken into consideration. The complexity of the etiology of IgAN requires comprehensive treatment and management. Our findings provide a new therapeutic approach involving the reconstruction of the intestinal microenvironment and maintenance of metabolic balance. Fecal microbiota transplantation (FMT) is rapidly emerging due to its safety and stability (40). As mentioned earlier, *Bacteroidetes*, one of the earliest colonizing and most abundant constituents of the intestinal flora that may induce an anti-inflammatory milieu (41), was found to be significantly lower among IgAN patients. Food supplements, pharmaceutical products, and FMT may be promising therapeutic approaches to re-establish stable *Bacteroidetes* levels. Also, fat and protein metabolism disorders in IgAN patients, especially polyunsaturated fatty acid deficiency, should be considered. Maintaining metabolic balance and homeostasis is an essential therapeutic priority. Previous studies have reported that n-3 and n-6 long-chain polyunsaturated fatty acid supplements had a positive therapeutic effect in type 2 diabetes mellitus and coronary heart disease patients (42,43). A reasonable diet and wise supplementation of polyunsaturated fatty acids are essential for the prevention and treatment of IgAN.

Our study had the following limitations. Accurately assessing fecal metabolites, most of which are affected by diet and lifestyle factors, and distinguishing host-derived metabolites from microbially-generated metabolites is exceptionally challenging. Our findings revealed a significant alteration in the gut microbiota and metabolic phenotypes of IgAN patients. However, to improve the accuracy and specificity of molecular diagnoses and to identify molecular biomarkers, in-depth research on the characteristics of the gut microbiota and relative metabolites associated with different types of glomerulonephritis will be necessary. Additionally, 16S rRNA techniques can be used to assess the relative abundance, but not the absolute abundance of the microbial community. Therefore, the observed dynamics may not accurately reflect actual taxon densities (44).

Conclusions

A shift in the relative abundance of some bacteria was observed in IgAN patients compared with HCs. The changes in gut microbiota also affected metabolism and the absorbance of specific fatty acids, particularly polyunsaturated fatty acids (5-HETE and 5-HETrE), free amino acids, and oligopeptides, resulting in a unique metabolic system in IgAN patients. Six metabolites were identified–bilirubin, trimethoprim, stearamide, phenylalanine, cis-9,10-epoxystearic acid, and PE lyso 17:0—that connected the metabolic networks of the gut and blood and might be pivotal metabolites for IgAN. The activation of the phenylalanine metabolism pathway should be further examined. Furthermore, we found that 5-HETE and 5-HETrE were associated with the classification of segmental sclerosis but not 24-hour proteinuria or eGFR. This comprehensive analysis of microbial metabolites provides more functional insights than any single dataset alone.

Acknowledgments

The authors thank the many volunteers who participated in the study and AME Editing (http://editing.amegroups.cn/)

for editing this manuscript.
Funding: This work was supported by the National Natural Science Foundation of China (No. 81671596), The National Science Foundation for Young Scientists of China (No. 31700795), The Education Innovation Project for Graduates of Guangzhou, China (No. 2020XLLT10), The Twenty-one Teaching Reform Project of Jinan University (No. JG2019044).

Footnote

Data Sharing Statement: Available at http://dx.doi.org/10.21037/atm-20-2506

Peer Review File: Available at http://dx.doi.org/10.21037/atm-20-2506

Conflicts of Interest: All authors have completed the ICMJE uniform disclosure form (available at http://dx.doi.org/10.21037/atm-20-2506). The authors have no conflicts of interest to declare.

Ethical Statement: The authors are accountable for all aspects of the work and ensuring that questions related to the accuracy or integrity of any part of the work are appropriately investigated and resolved. The present study was conducted following the principles of the Declaration of Helsinki (as revised in 2013) and was authorized by the ethics board of Shenzhen People's Hospital (LL-KY-2019514). All participating individuals provided signed informed consent.

References

1. Li LS, Liu ZH. Epidemiologic data of renal diseases from a single unit in China: analysis based on 13,519 renal biopsies. Kidney Int 2004;66:920-3.
2. D'Amico G. Natural history of idiopathic IgA nephropathy and factors predictive of disease outcome. Semin Nephrol 2004;24:179-96.
3. Robert T, Berthelot L, Cambier A, et al. Molecular insights into the pathogenesis of IgA nephropathy. Trends Mol Med 2015;21:762-75.
4. Chen A, Yang SS, Lin TJ, et al. IgA nephropathy: clearance kinetics of IgA-containing immune complexes. Semin Immunopathol 2018;40:539-43.
5. Kiryluk K, Novak J. The genetics and immunobiology of IgA nephropathy. J Clin Invest 2014;124:2325-32.
6. Wyatt RJ, Julian BA. IgA nephropathy. N Engl J Med 2013;368:2402-14.
7. Piccolo M, De Angelis M, Lauriero G, et al. Salivary microbiota associated with immunoglobulin A nephropathy. Microb Ecol 2015;70:557-65.
8. Floege J, Feehally J. The mucosa–kidney axis in IgA nephropathy. Nat Rev Nephrol 2016;12:147.
9. De Angelis M, Montemurno E, Piccolo M, et al. Microbiota and metabolome associated with immunoglobulin A nephropathy (IgAN). PLoS One 2014;9:e99006.
10. McCarthy DD, Kujawa J, Wilson C, et al. Mice overexpressing BAFF develop a commensal flora–dependent, IgA-associated nephropathy. J Clin Invest 2011;121:3991-4002.
11. Marcobal A, Kashyap PC, Nelson T, et al. A metabolomic view of how the human gut microbiota impacts the host metabolome using humanized and gnotobiotic mice. ISME J 2013;7:1933-43.
12. Mishima E, Fukuda S, Mukawa C, et al. Evaluation of the impact of gut microbiota on uremic solute accumulation by a CE-TOFMS–based metabolomics approach. Kidney Int 2017;92:634-45.
13. Sabatino A, Regolisti G, Brusasco I, et al. Alterations of intestinal barrier and microbiota in chronic kidney disease. Nephrol Dial Transplant 2015;30:924-33.
14. Levey AS, Stevens LA, Schmid CH, et al. A new equation to estimate glomerular filtration rate. Ann Intern Med 2009;150:604-12.
15. Stevens LA, Schmid CH, Zhang YL, et al. Development and validation of GFR-estimating equations using diabetes, transplant and weight. Nephrol Dial Transplant 2010;25:449-57.
16. Magoč T, Salzberg SL. FLASH: fast length adjustment of short reads to improve genome assemblies. Bioinformatics 2011;27:2957-63.
17. Bolger AM, Lohse M, Usadel B. Trimmomatic: a flexible trimmer for Illumina sequence data. Bioinformatics

2014;30:2114-20.
18. Edgar RC, Haas BJ, Clemente JC, et al. UCHIME improves sensitivity and speed of chimera detection. Bioinformatics 2011;27:2194-200.
19. Edgar RC. UPARSE: highly accurate OTU sequences from microbial amplicon reads. Nat Methods 2013;10:996-8.
20. Wang Q, Garrity GM, Tiedje JM, et al. Naive Bayesian classifier for rapid assignment of rRNA sequences into the new bacterial taxonomy. Appl Environ Microbiol 2007;73:5261-7.
21. Quast C, Pruesse E, Yilmaz P, et al. The SILVA ribosomal RNA gene database project: improved data processing and web-based tools. Nucleic Acids Res 2013;41:D590-6.
22. Caporaso JG, Bittinger K, Bushman FD, et al. PyNAST: a flexible tool for aligning sequences to a template alignment. Bioinformatics 2010;26:266-7.
23. Schloss PD, Westcott SL, Ryabin T, et al. Introducing mothur: open-source, platform-independent, community-supported software for describing and comparing microbial communities. Appl Environ Microbiol 2009;75:7537-41.
24. Adusumilli R, Mallick P. Data conversion with ProteoWizard msConvert. Methods Mol Biol 2017;1550:339-68.
25. Wiklund S, Johansson E, Sjöström L, et al. Visualization of GC/TOF-MS-based metabolomics data for identification of biochemically interesting compounds using OPLS class models. Anal Chem 2008;80:115-22.
26. Trygg J, Wold S. Orthogonal projections to latent structures (O-PLS). J Chemom 2002;16:119-28.
27. Nallu A, Sharma S, Ramezani A, Muralidharan J, Raj D. Gut microbiome in chronic kidney disease: challenges and opportunities. Transl Res 2017;179:24-37.
28. Kasubuchi M, Hasegawa S, Hiramatsu T, et al. Dietary gut microbial metabolites, short-chain fatty acids, and host metabolic regulation. Nutrients 2015;7:2839-49.
29. Sánchez B, Delgado S, Blanco-Míguez A, et al. Probiotics, gut microbiota, and their influence on host health and disease. Mol Nutr Food Res 2017;61:1600240.
30. D'Argenio V, Salvatore F. The role of the gut microbiome in the healthy adult status. Clin Chim Acta 2015;451:97-102.
31. Goodrich JK, Waters JL, Poole AC, et al. Human genetics shape the gut microbiome. Cell 2014;159:789-99.
32. Schmitt R, Carlsson F, Mörgelin M, et al. Tissue deposits of IgA-binding streptococcal M proteins in IgA nephropathy and Henoch-Schönlein purpura. Am J Pathol 2010;176:608-18.
33. Han L, Fang X, He Y. ISN forefronts symposium 2015: IgA nephropathy, the gut microbiota, and gut-kidney crosstalk. Kidney Int Rep 2016;1:189-96.
34. Meijers BK, Evenepoel P. The gut–kidney axis: indoxyl sulfate, p-cresyl sulfate and CKD progression. Nephrol Dial Transplant 2011;26:759-61.
35. Bammens B, Verbeke K, Vanrenterghem Y, et al. Evidence for impaired assimilation of protein in chronic renal failure. Kidney Int 2003;64:2196-203.
36. An WS, Kim HJ, Cho KH, et al. Omega-3 fatty acid supplementation attenuates oxidative stress, inflammation, and tubulointerstitial fibrosis in the remnant kidney. Am J Physiol Renal Physiol 2009;297:F895-903.
37. Wang S, Lv D, Jiang S, et al. Quantitative reduction in short-chain fatty acids, especially butyrate, contributes to the progression of chronic kidney disease. Clin Sci (Lond) 2019;133:1857-70.
38. Chen YY, Chen DQ, Chen L, et al. Microbiome–metabolome reveals the contribution of gut–kidney axis on kidney disease. J Transl Med 2019;17:5.
39. Mafra D, Barros AF, Fouque D. Dietary protein metabolism by gut microbiota and its consequences for chronic kidney disease patients. Future Microbiol 2013;8:1317-23.
40. Vindigni SM, Surawicz CM. Fecal Microbiota Transplantation. Gastroenterol Clin North Am 2017;46:171-85.
41. Xu M, Xu X, Li J, et al. Association between gut microbiota and autism spectrum disorder: A systematic review and meta-analysis. Front Psychiatry 2019;10:473-86.
42. Forouhi NG, Imamura F, Sharp SJ, et al. Association of plasma phospholipid n-3 and n-6 polyunsaturated fatty acids with type 2 diabetes: The EPIC-InterAct Case-Cohort Study. PLoS Med 2016;13:e1002094.
43. Bird JK, Calder PC, Eggersdorfer M. The role of n-3 long chain polyunsaturated fatty acids in cardiovascular disease prevention, and interactions with statins. Nutrients 2018;10:775.
44. Props R, Kerckhof FM, Rubbens P, et al. Absolute quantification of microbial taxon abundances. ISME J 2017;11:584-7.

Cite this article as: Wu H, Tang D, Zheng F, Li S, Zhang X, Yin L, Liu F, Dai Y. Identification of a novel interplay between intestinal bacteria and metabolites in Chinese patients with IgA nephropathy via integrated microbiome and metabolome approaches. Ann Transl Med 2021;9(1):32. doi: 10.21037/atm-20-2506

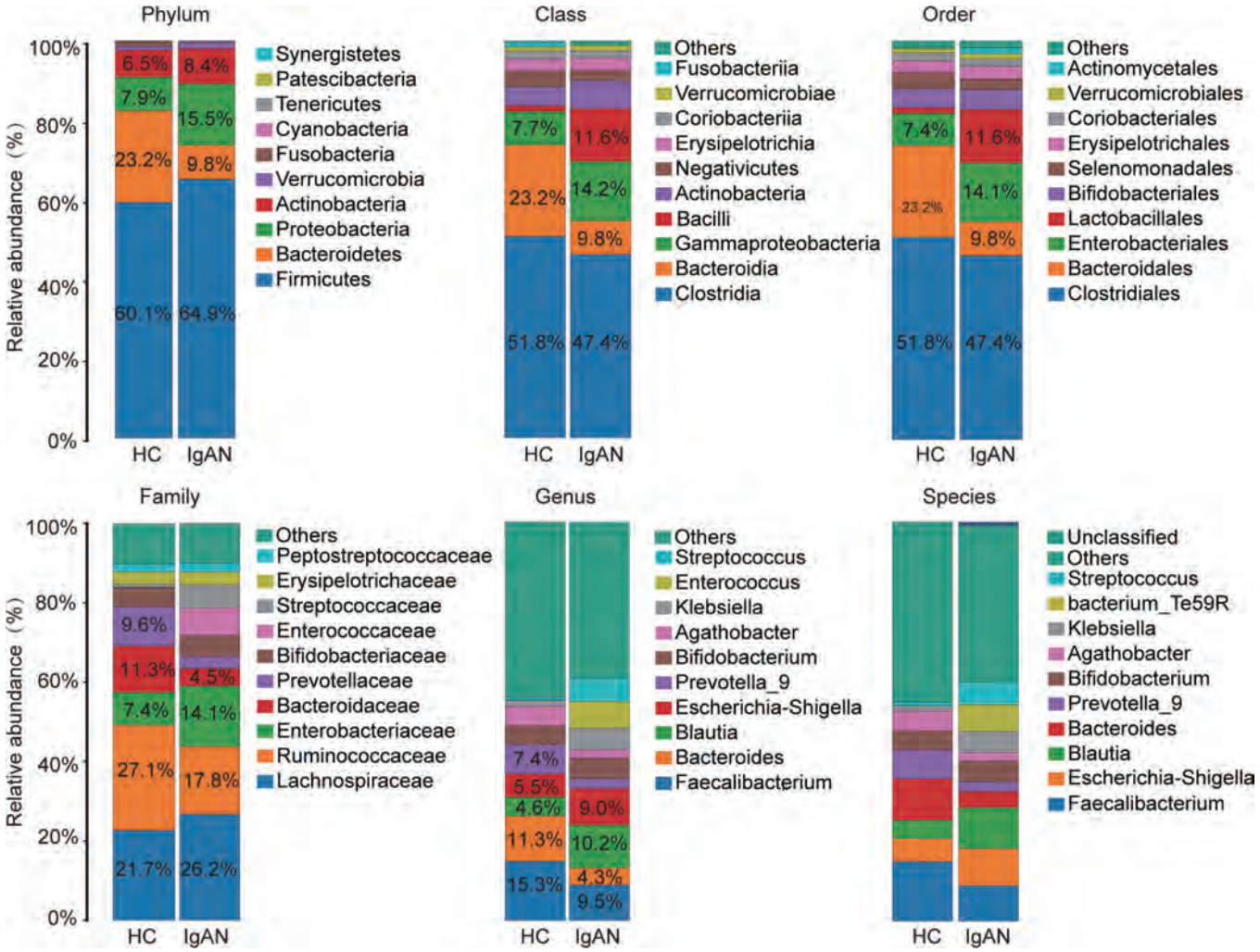

Figure S1 Relative abundance analysis of gut microbiota. Change in relative abundance (%) of bacteria in fecal samples from immunoglobulin A nephropathy (IgAN) and healthy control (HC) groups at different levels of biologic classification (phylum, class, order, family, genus, species).

http://dx.doi.org/10.21037/atm-20-2506

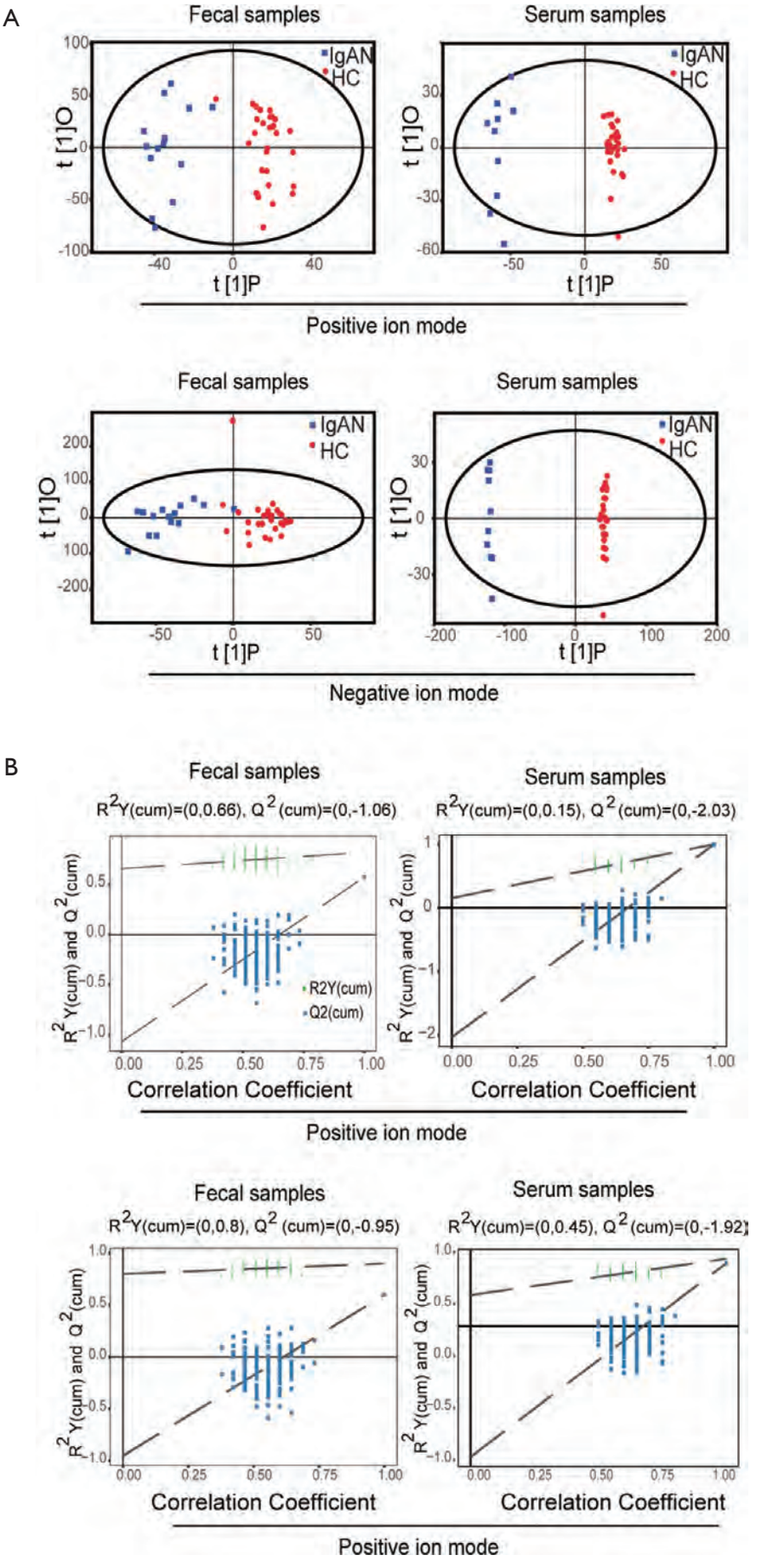

Figure S2 Differences in metabolic profile between healthy controls (HCs) and immunoglobulin A nephropathy (IgAN) patients. Orthogonal projections to latent structures-discriminant analysis (OPLS-DA) score plots (A) and permutation tests of OPLS-DA models (B) for fecal and serum samples from HC and IgAN groups. To assess the robustness and predictive ability of the OPLS-DA model, 200 permutations were conducted, and R2 and Q2 intercept values were obtained. R2 indicates how well the variation of each variable is explained. Q2 intercept value represents the robustness of the model, the risk of overfitting, and the reliability of the model, with lower values indicating better models. Results indicate that the model was robust without overfitting.

http://dx.doi.org/10.21037/atm-20-2506

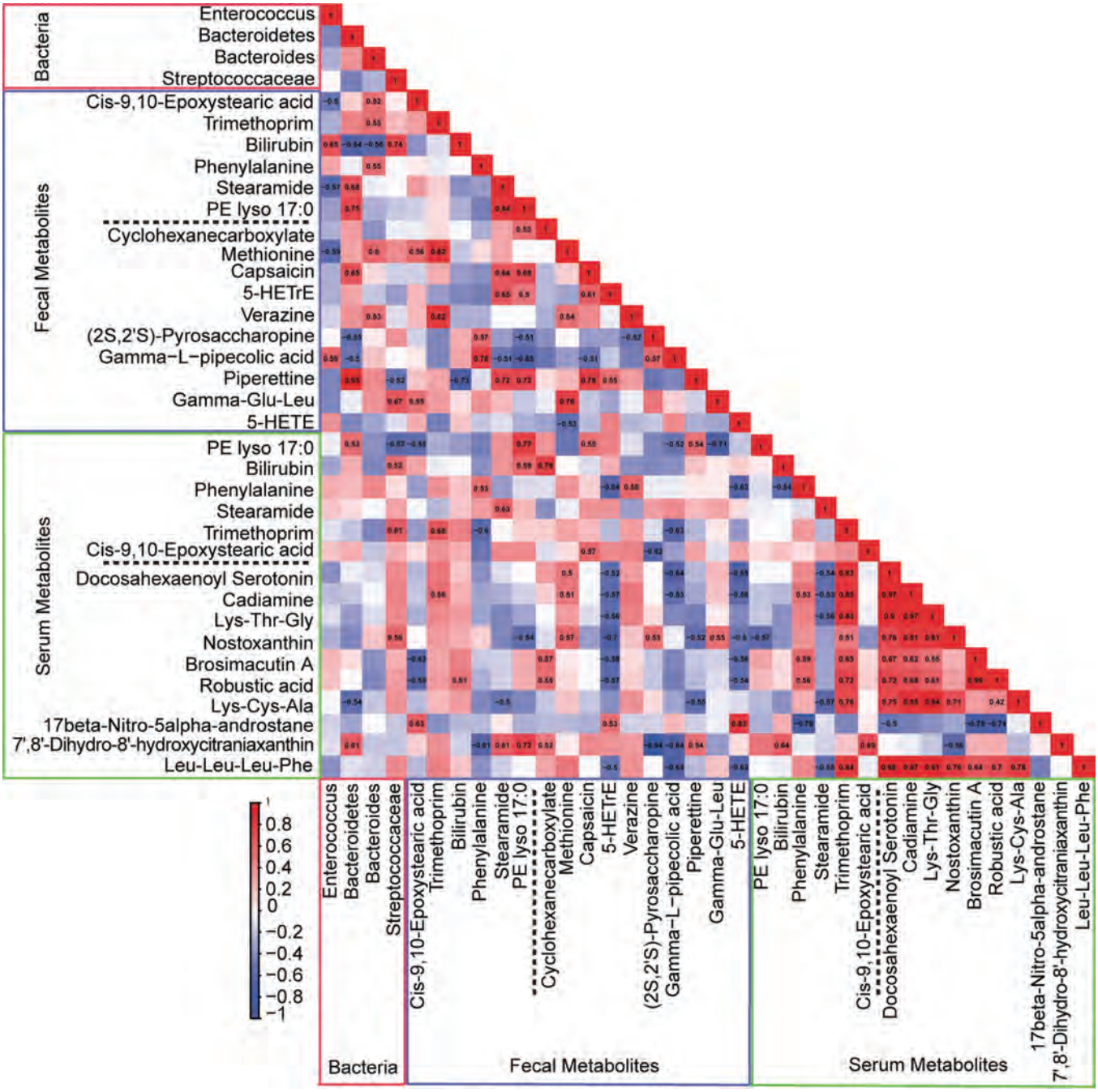

Figure S3 Correlation between fecal microbes, fecal metabolites, and serum metabolites in immunoglobulin A nephropathy patients. Correlation coefficients $|r|>0.5$ and $P<0.05$ are marked with numbers and considered significant correlations. r, Pearson correlation coefficient.

http://dx.doi.org/10.21037/atm-20-2506

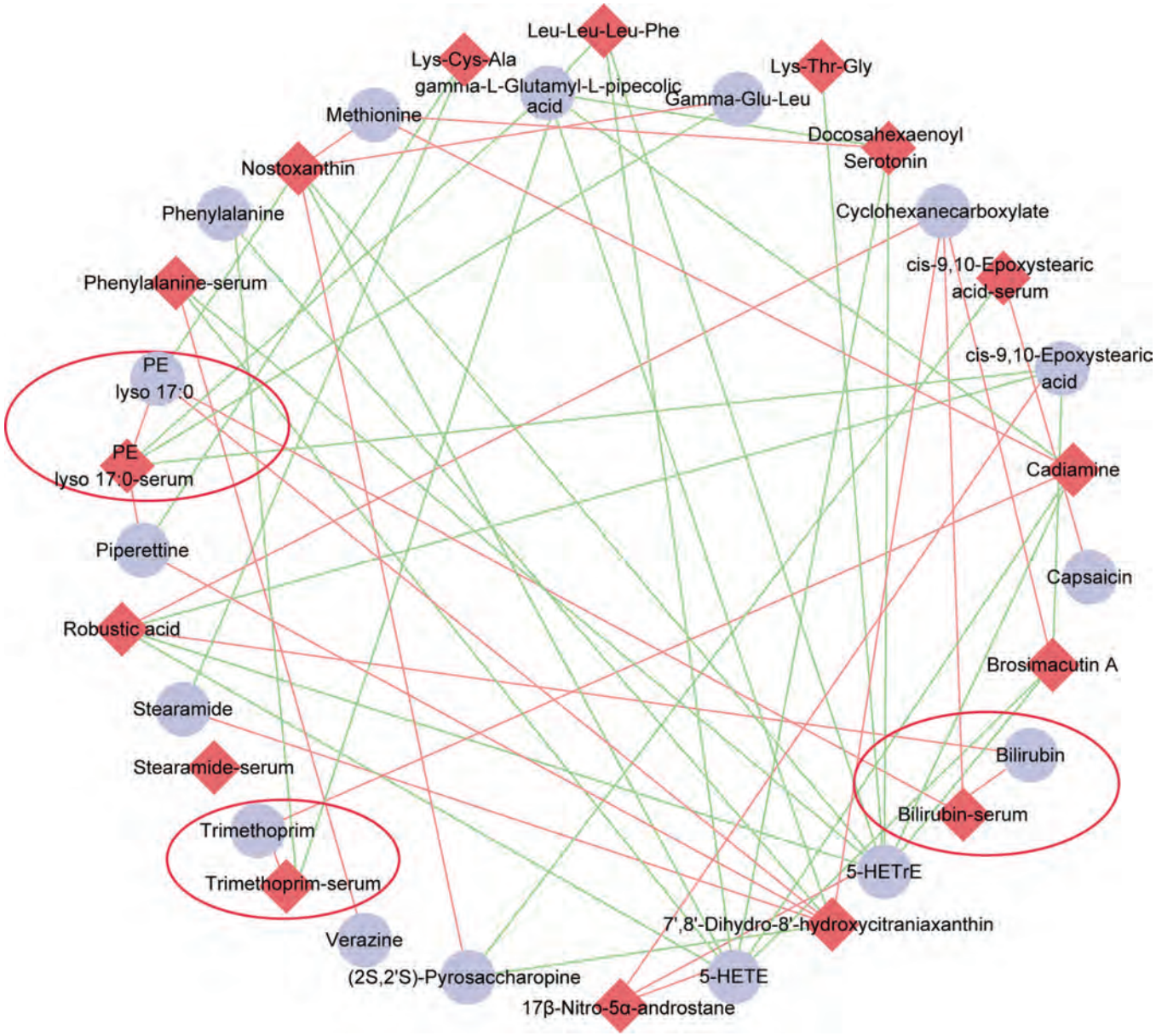

Figure S4 Correlation between fecal metabolites and serum metabolites in immunoglobulin A nephropathy patients (|r|>0.5). The rhombus represents serum metabolites, and the circles represent fecal metabolites. Green lines indicate negative correlations, and red lines represent positive correlations. r, Pearson correlation coefficient.

http://dx.doi.org/10.21037/atm-20-2506

Table S1 Clinical characteristics of healthy controls and immunoglobulin A nephropathy patients

	Healthy control group n=30	IgAN group n=15
Gender (male/female)	20/10	7/8
Age (years)	44.1±1.91	38.64±2.91
BMI (kg/m^2)	24.54±0.78	21.89±0.72
Systolic pressure	125.6±4.335	118.9±3.241
24h proteinuria	NA	1.94±0.44
ALT(U/L)	24.55±2.08	14±1.64
AST(U/L)	22.2±0.92	19.36±1.25
Serum albumin(g/L)	44.76±0.56	33.41±2.29***
FBG (mmol/l)	5.379±0.13	5.027±0.17
Urea nitrogen(mmol/l)	4.78±0.23	6.16±0.97
Creatinine(umol/l)	75.43±3.24	168.7±61.26*
Uric acid(umol/l)	339.5±15.65	435.5±37.07**
cholesterol(mmol/l)	4.56±0.15	5.56±0.66
Triglyceridemmol/l	1.51±0.24	1.3±0.14
HDL (mmol/l)	1.46±0.05	1.16±0.12
LDL (mmol/l)	2.47±0.11	3.21±0.38

BMI, Body Mass Index; ALT, alanine transaminase; AST, aspartate amino transferase; FBG, fasting blood glucose; HDL, high density lipoprotein; LDL, low density lipoprotein; NA, not available. *, P<0.05; **, P<0.01; ***, P<0.001

Table S2 Histological characteristics of immunoglobulin A nephropathy patients

Patients	Glomerular number	Endocapillary proliferation	Segmental sclerosis	Mesangial hypercellularity	Tubular atrophy	Crescent	Interstitial fibrosis	Inflammatory infiltration	IgG	IgA	IgM	C1q	C3	Oxford classification
No.1	30	√	√	>50%	35%	5%	+	++	−	+++	+	−	+	M1S1E1T1C1
No.2	37	√	√	>50%	65%	2%	++	+++	−	+++	-	−	−	M1S1E1T2C1
No.3	23	√	×	<50%	10%	0%	+	+	+	+++	+	−	−	M0S0E1T0C0
No.4	16	√	×	>50%	20%	0%	++	+++	−	+++	−	−	++	M1S0E1T0C0
No.5	19	×	×	<50%	10%	0%	−	+	−	+++	−	−	−	M0S0E0T0C0
No.6	15	×	√	>50%	30%	0%	++	++	−	+++	−	−	−	M1S1E0T1C0
No.7	10	×	×	<50%	10%	0%	++	++	−	++	−	−	−	M0S0E0T0C0
No.8	18	×	√	<50%	20%	0%	+	+	+	++	−	−	−	M0S1E0T0C0
No.9	22	√	×	>50%	60%	6%	++	++	−	++	+	−	−	M1S0E1T2C1
No.10	15	√	×	<50%	10%	0%	+	+	−	+++	+	−	++	M0S0E1T0C0
No.11	20	×	√	<50%	5%	0%	+	+	−	+++	−	−	++	M0S1E0T0C0
No.12	26	×	√	>50%	40%	0%	+	+	−	+++	−	−	−	M1S1E0T1C0
No.13	14	√	√	<50%	36%	0%	++	++	+	+++	−	−	++	M0S1E1T1C0
No.14	15	×	√	>50%	28%	0%	++	+	−	++	−	−	++	M1S1E0T1C0
No.15	27	√	×	<50%	18%	0%	+	+	+	+++	−	−	+	M0S0E1T0C0

(–), Negative result; (+), varying degrees.

http://dx.doi.org/10.21037/atm-20-2506

Table S3 Differential metabolites in the fecal samples of the healthy control and immunoglobulin A nephropathy groups

MS2 name	Log FC	Classification	Ionization mode
Evoxanthidine	–2.24	Acridines	POS
O-propanoyl-carnitine	–1.91	Acylcarnitine	POS
1,7-Dimethyluric acid	–2.72	Alkaloid	POS
Capsaicin	–4.75	Alkaloid	POS
Cassaine	–3.17	Alkaloid	POS
Codeine	–1.96	Alkaloid	POS
Piperettine	–4.63	Alkaloid	POS
Verazine	–3.86	Alkaloid	POS
Suloctidil	–2.35	Amines	NEG
Methionine	1.67	Amino acid	POS
L-Methionine	0.93	Amino acid	NEG
Lysine	0.88	Amino acid	NEG
Phenylalanine	1.19	Amino acid	NEG
Rebamipide	–2.33	Amino acid	POS
trans-S-(1-Propenyl)-L-cysteine	–2.98	Amino acid derivative	POS
Trimethoprim	1.83	Aminopyrimidine	POS
Isoxaben	–1.68	Benzazole	POS
Raclopride	–3.02	Benzazole	POS
3-Indolepropionic acid	–1.36	Benzazole	NEG
Boviquinone 4	–1.10	Benzoquinone	POS
beta-L-Fucose 1-phosphate	–3.45	Carbohydrate	NEG
Bufalin	–2.66	Carbohydrate	NEG
D-Glucuronic acid	1.09	Carbohydrate	NEG
Xanthosine	0.71	Carbohydrate	NEG
(2S,2'S)-Pyrosaccharopine	4.33	Carbohydrate	POS
THTC	1.26	Carboxylic Acids	POS
3,4-Dimethoxycinnamic acid	–4.70	Carboxylic Acids	NEG
3-Phenylpropionic acid	–2.46	Carboxylic Acids	NEG
alpha-CMBHC	–1.16	Carboxylic Acids	NEG
Mycophenolic acid	–1.14	Carboxylic Acids	NEG
Norleucine	1.07	Carboxylic Acids	NEG
Sebacic acid	–1.11	Carboxylic Acids	NEG
Urocanate	1.24	Carboxylic Acids	NEG
Aspidofractine	–1.40	Carboxylic Acids	POS
3,6-Dioxo-5beta-cholan-24-oic Acid	–2.98	Cholic Acids	POS
3-Oxo-5beta-chola-7,9(11)-dien-24-oic Acid	–3.02	Cholic Acids	POS
3b-Hydroxy-5-cholenoic acid	–1.63	Cholic Acids	NEG
Dronedarone	–1.65	Cytochrome	NEG
Deoxycholate	–0.69	Eoxycholic acid	NEG
Ursodeoxycholic acid	–1.07	Eoxycholic acid	POS
Erythronolactone	0.53	Esters	NEG
delta-Tridecalactone	–2.74	Esters	POS
(3b,24x)-Cycloartane-3-oxo-24,25-diol	3.65	Fatty Alcohols	POS
13-Tetradecene-1,3-diyne-6,7-diol	–0.81	Fatty Alcohols	POS
Falcarindiol	–0.83	Fatty Alcohols	POS
15-HETE-DA	–0.97	Fatty amides	POS
N-docosanoyl taurine	–2.67	Fatty amides	POS
N-oleoyl phenylalanine	–2.02	Fatty amides	POS
Palmitoleamide	–2.63	Fatty amides	POS
Stearamide	–1.66	Fatty amides	POS
(4Z,7Z,10Z,13Z,16Z,19Z)-Docosahexaenoic acid ethyl ester	–1.10	Fatty esters	POS
4E-Decenyl acetate	–2.36	Fatty esters	POS
Stearidonic Acid ethyl ester	–2.17	Fatty esters	POS
29-Norcycloartane-3,24-dione	–1.35	Flavonoids	POS
1-Hydroxy-2-(9Z,12Z-octadecadienoyl)-sn-glycero-3-phosphoethanolamine	–1.50	Phospholipid	NEG
PE(18:1(9Z)/0:0)	–0.79	Phospholipid	NEG
Phosphatidylethanolamine lyso 17:0	0.98	Phospholipid	NEG
PE(O-16:0/0:0)	–1.08	Phospholipid	POS
Enterolactone	–1.50	Hydrocarbon	NEG
Maslinic Acid	–1.45	Hydrocarbon	NEG
5-(1-hydroxypropan-2-yl)isolongifolane	–2.71	Hydrocarbon	POS
5-propylideneisolongifolane	–2.77	Hydrocarbon	POS
Cassaidine	–1.15	Hydrocarbon	POS
2-(5,8-Tetradecadienyl)cyclobutanone	–1.80	Ketosteroid	POS
3-keto Petromyzonol	–0.78	Ketosteroid	POS
12,13-DiHOME	–1.46	Long-chain fatty acid	NEG
15S-HEPE	–1.75	Long-chain fatty acid	NEG
16R-HETE	–1.05	Long-chain fatty acid	NEG
17-Octadecynoic Acid	–2.24	Long-chain fatty acid	NEG
2,3-dinor Thromboxane B1	–1.03	Long-chain fatty acid	NEG
3-hydroxy-tetradecanoic acid	–1.33	Long-chain fatty acid	NEG
5-HETE	–2.69	Long-chain fatty acid	NEG
5-HETrE	–4.67	Long-chain fatty acid	NEG
9,10-DiHOME	–1.19	Long-chain fatty acid	NEG
9R,10S-EpOME	–1.88	Long-chain fatty acid	NEG
alpha-ESA	–2.00	Long-chain fatty acid	NEG
Arachidonic Acid	–1.00	Long-chain fatty acid	NEG
cis-9,10-Epoxystearic acid	–1.82	Long-chain fatty acid	NEG
DL-2-hydroxy stearic acid	–2.33	Long-chain fatty acid	NEG
Eicosapentaenoic Acid	–1.41	Long-chain fatty acid	NEG
Oleic acid	–0.93	Long-chain fatty acid	NEG
Palmitoleic acid	–1.69	Long-chain fatty acid	NEG
11beta-PGF2alpha	–2.56	Long-chain fatty acid	POS
12(R)-HEPE	–2.08	Long-chain fatty acid	POS
17-phenyl trinor PGF2alpha cyclohexyl amide	–1.13	Long-chain fatty acid	POS
9,10-epoxy-11-hydroxy-12-octadecenoic acid	–1.70	Long-chain fatty acid	POS
Myristoleic acid	–2.74	Long-chain fatty acid	POS
13,14-dehydro-15-cyclohexyl Carbaprostacyclin	–1.19	Long-chain fatty acid	NEG
15(R)-Iloprost	–1.62	Long-chain fatty acid	NEG
16,16-dimethyl-PGA1	–0.35	Long-chain fatty acid	NEG
FAHFA 36:1	–1.68	Long-chain fatty acid	NEG
14,15-EE-8(Z)-E	–2.30	Other	NEG
1,2-Dihydroxytacrine	–1.39	Other	POS
Cadabicilone	–1.69	Other	POS
Schidigeragenin B	–1.17	Other	POS
Potassium bis(2-hydroxyethyl)dithiocarbamate	–1.19	Other	POS
6-Hydroxymethyletoricoxib	–1.32	Oxidoreductase	POS
Isoquinoline N-oxide	–0.89	Oxynitride	NEG
Gamma-Glu-Leu	1.77	Peptide	NEG
Met-Met-Pro	–1.81	Peptide	POS
Trp-Val-Val	–2.35	Peptide	POS
Ile-Gly-Ile	1.41	Peptide	POS
Leu-Ser-Asn-His	–1.04	Peptide	POS
Lys-Gly-Leu	2.45	Peptide	POS
Met-Tyr-Arg	1.57	Peptide	POS
Thr-Phe	0.89	Peptide	POS
Tyr-OEt	–1.54	Peptide	POS
Val-Asn-Ile	1.44	Peptide	POS
Val-Ser-Val	1.26	Peptide	POS
Acetyl-DL-Valine	–2.59	Peptide	POS
LPA(0:0/16:0)	–2.98	Phosphatidic acids	POS
PE(18:2(9Z,12Z)/0:0)	–2.20	Phosphatidic acids	POS
PC(14:0/O-1:0)	–1.53	Phosphocholine	POS
Bilirubin	0.97	Pigment	POS
Mesobilirubinogen	1.57	Pigment	POS
gamma-L-Glutamyl-L-pipecolic acid	5.09	Pipecolic acid	POS
PGG2	–2.60	Prostanoid	NEG
19(R)-hydroxy PGF2alpha	–1.70	Prostanoid	POS
PGH1	–1.82	Prostanoid	POS
Adenine	–0.64	Purines	NEG
Valganciclovir	–2.07	Purines	NEG
D-erythro-Sphingosine C-20	–1.46	Sphingosine	POS
3alpha,12alpha-Dihydroxy-5beta-pregnan-20-one diacetate	–0.94	Steroid	POS
6-keto Testosterone Enanthate	–1.18	Steroid	POS
Quercetin Pentamethyl Ether	–1.68	Steroid	POS
(22E)-3alpha,12alpha-Dihydroxy-5beta-chol-22-en-24-oic Acid	–1.15	Sterol Lipids	POS
25-Hydroxy[26,27-methyl]vitamin D3 3beta-(1,2-epoxypropyl)ether	–1.27	Sterol Lipids	POS
7,12-Dioxo-5beta-cholan-24-oic Acid	–0.85	Sterol Lipids	POS
Crassin acetate	2.25	Terpene	POS
1alpha,25-dihydroxy-8(14)a-homovitamin D3	–1.88	Vitamins	POS

A total of 131 differential metabolites were identified, including 78 metabolites in positive ion mode and 53 metabolites in negative ion mode. The following screening criteria were set: VIP >1 and P<0.05. Compared to the HC group, a total of 110 metabolites were lower and 21 metabolites were higher in the IgAN group. We also classified each metabolite based on its chemical properties. HC, healthy control; IgAN, immunoglobulin A nephropathy; Log FC, Log fold change; POS, positive ion mode; NEG, negative ion mode.

http://dx.doi.org/10.21037/atm-20-2506

Table S4 Differential metabolites in the serum samples of the healthy control and immunoglobulin A nephropathy groups

MS2 name	Log FC	Classification	Ionization mode
Pseudopelletierine	8.31	Alkaloids	POS
Gabapentin	7.26	Amines	POS
Cadiamine	11.97	Amines	POS
Selenohomocysteine	1.86	Amino acid zwitterion	POS
Tryptophan	0.46	Amino acid	NEG
D-Glu	0.43	Amino acid	NEG
Arginine	0.45	Amino acid	NEG
Phenylalanine	0.30	Amino acid	NEG
7',8'-Dihydro-8'-hydroxycitraniaxanthin	–9.21	Benzopyrans	POS
Pseudouridine	–0.49	Carbohydrate	NEG
L-(+)-Gulose	0.35	Carbohydrate	NEG
L-Erythrulose	0.22	Carbohydrate	NEG
D-Lactic acid	–0.39	Carboxylic acid	NEG
Pyroglutamic acid	–0.35	Carboxylic acid	NEG
Pyruvic acid	–0.32	Carboxylic acid	NEG
PSOROMIC ACID	0.08	Carboxylic acid	NEG
Thiofanox	–8.89	Carboxylic acid	POS
3-Phenoxybenzoic acid	–0.25	Carboxylic acid	NEG
Glycocholic Acid	–5.12	Cholic Acids	POS
Deoxycholic acid	–1.75	Eoxycholic acid	NEG
Isohyodeoxycholic acid	–1.65	Eoxycholic acid	NEG
4-Methoxycinnamoyloleanolic acid methyl ester	–4.59	Esters	POS
Oleamide	–6.30	Fatty amide	POS
Stearamide	–5.13	Fatty amide	POS
dodecanamide	–0.63	Fatty amide	POS
C-6 NBD-dihydro-Ceramide	–7.20	Fatty amide	POS
2-(4-Morpholinyl)benzothiazole	–7.74	Flavonoids	POS
N-docosahexaenoyl GABA	–1.54	Flavonoids	POS
PE(16:1(5Z)/16:1(5Z))	–8.49	Glycerophospholipid	POS
Irbesartan	–1.29	Hydrocarbon	NEG
Confertifoline	–2.31	Hydrocarbon	NEG
2-tetracosanamidoethanesulfonic acid	–2.01	Hydrocarbon	NEG
(-)-Perillic acid	–2.37	Hydrocarbon	NEG
Sclerosporin	–1.11	Hydrocarbon	POS
Dihydrovaltrate	–5.41	Hydrocarbon	POS
Nostoxanthin	–9.30	Hydrocarbon	POS
Robustic acid	10.69	Hydroxy compound	POS
Docosahexaenoyl Serotonin	12.13	Indoles	POS
Sunitinib	–0.84	Indoles	NEG
3,4-Dehydro-6-hydroxymellein	–0.46	Lactones	POS
13-HpODE	–0.58	Lipid Peroxides	NEG
9-HETE	–1.58	Long-chain fatty acid	NEG
13-HODE	–1.27	Long-chain fatty acid	NEG
12-OPDA	0.53	Long-chain fatty acid	NEG
Palmitic amide	–5.16	Long-chain fatty acid	POS
Oleoyl Ethyl Amide	–4.04	Long-chain fatty acid	POS
Isolauric acid	–0.60	Medium-chain fatty acid	NEG
Lauric acid	–0.17	Medium-chain fatty acid	NEG
Undecanoic acid	–0.09	Medium-chain fatty acid	NEG
Decanoic acid	–0.45	Medium-chain fatty acid	NEG
cis-9,10-Epoxystearic acid	–0.88	Medium-chain fatty acid	NEG
cis-5-dodecenoic acid	–0.96	Medium-chain fatty acid	NEG
Dihydrojasmonic Acid	–0.14	Medium-chain fatty acid	NEG
Myristic Acid Alkyne	–1.47	Medium-chain fatty acid	NEG
Trimethoprim	3.77	Miazines	POS
Dodecylbenzenesulfonic acid	–0.24	Organic acid	NEG
Lys-Thr-Gly	10.44	Peptide	POS
Lys-Cys-Ala	11.69	Peptide	POS
Leu-Val-Lys-Arg	–2.73	Peptide	POS
Brosimacutin A	13.22	Peptide	POS
Leu-Leu-Phe	13.53	Peptide	POS
Leu-Pro-Leu-Lys	–8.09	Peptide	POS
Acylated phloroglucinol	9.13	Phenols	NEG
Phenolphthalein	–0.11	Phenols	NEG
4-Hexylresorcinol	–2.03	Phenols	NEG
PC(18:2(9Z,12Z)/12:0)	–7.01	Phosphocholine	POS
PC(0:0/14:0)	–8.09	Phosphocholine	POS
PC(P-19:1(12Z)/0:0)	–9.20	Phosphocholine	POS
Phosphatidylethanolamine lyso 16:0	0.60	Phospholipids	NEG
Phosphatidylethanolamine lyso 17:0	0.72	Phospholipids	NEG
Phosphatidylinositol 16:0-18:2	0.62	Phospholipids	NEG
Bilirubin	1.41	Pigment	POS
6-(Methylthio)purine	–0.38	Purines	NEG
N-Methyl-2-pyrrolidinone	4.58	Pyrrolidinones	POS
Isokobusone	–0.33	Steroid	NEG
3-beta-hydroxyandrost-5-en-17-one sulfate	–0.99	Steroid	NEG
NORETHINDRONE ACETATE	–0.71	Steroid	NEG
17beta-Nitro-5alpha-androstane	–11.29	Steroid	POS
17-[(Benzylamino)methyl]estra-1,3,5(10)-triene-3,17beta-diol	9.21	Steroid	POS
(23R)-23,25-dihydroxyvitamin D3	–0.59	Vitamin	NEG

Eighty differential metabolites were identified, including 43 metabolites in positive ion mode and 37 metabolites in negative ion mode. The following screening criteria were set: VIP >1 and P<0.05. Compared to the HC group, a total of 56 metabolites were lower and 24 metabolites were higher in the IgAN group. HC, healthy control; IgAN, immunoglobulin A nephropathy; Log FC, Log fold change; POS, positive ion mode; NEG, negative ion mode.

http://dx.doi.org/10.21037/atm-20-2506

Table S5 Correlation between intestinal microbes and metabolites in immunoglobulin A nephropathy patients

Bacteria	Fecal metabolites	Serum metabolites
Enterococcus	Cis-9,10-Epoxystearic acid	
	Bilirubin	
	Stearamide	
	Methionine	
	Gamma-L-Glutamyl-L-pepecolic acid	
Bacteroidetes	Bilirubin	7',8'-Dihydro-8'-hydroxycitraniaxanthin
	Stearamide	Lys-Cys-Ala
	PE lyso 17:0	PE lyso 17:0
	Capsaicin	
	(2S,2'S)-Pyrosaccharopine	
	Gamma-L-Glutamyl-L-pepecolic acid	
	Piperettine	
Bacteroides	Cis-9,10-Epoxystearic acid	
	Trimethoprim	
	Bilirubin	
	Phenylalanine	
	Methionine	
	Verazine	
Streptococcaceae	Bilirubin	Bilirubin
	Piperettine	PE lyso 17:0
	Gamma-Glu-Leu	Trimethoprim
		Nostoxanthin

http://dx.doi.org/10.21037/atm-20-2506

Table S6 Correlation between intestinal microbes and metabolites in immunoglobulin A nephropathy patients

Bacteria	$Pro_{/24h}$<1.5g/L	$Pro_{/24h}$>1.5g/L	eGFR<90 mL/min/1.73 $^{m}2$	eGFR>90 mL/min/1.73 m^2
Streptococcus	1901±927.8	3454±2058	4259±1984	613.4±158
Bacteroides	1891±1060	2131±831.1	2298±810.5	1624±1075
Enterococcus	75±45.16	31.88±6.45	55.29±26.36	33.6±7.78
fecal metabolite				
gamma-L-Glutamyl-L-pipecolic acid	56.7±28.78	121.8±70.71	64.18±23.41	147.4±113.5
(2S,2'S)-Pyrosaccharopine	2.27±0.86	6.94±2.46	3.54±1.2	7.46±3.76
11beta-PGF2alpha	0.28±0.17	0.4±0.26	0.26±0.13	0.578±0.41
PGG2	0.2±0.14	0.3±0.17	0.3±0.17	0.19±0.09
Cyclohexanecarboxylate	0.36±0.27	0.28±0.17	0.28±0.18	0.37±0.27
5-HETE	0.37±0.18	0.11±0.03	0.28±0.12	0.12±0.04
Verazine	0.05±0.03	0.06±0.04	0.04±0.02	0.09±0.06
Piperettine	0.01±0.01	0.03±0.01	0.02±0.01	0.03±0.02
5-HETrE	0.11±0.06	0.10±0.05	0.09±0.04	0.13±0.09
Capsaicin	0.02±0.02	0.19±0.11	0.06±0.02	0.22±0.19
Serum metabolite				
Leu-Leu-Phe	2.42±0.49	2.77±0.28	2.52±0.34	2.84±0.35
Brosimacutin A	0.14±0.04	0.16±0.02	0.14±0.03	0.18±0.02
Docosahexaenoyl Serotonin	0.07±0.01	0.08±0.01	0.07±0.01	0.08±0.01
Cadiamine	3.58±0.65	3.73±0.34	3.63±0.43	3.74±0.44
Lys-Cys-Ala	0.05±0.01	0.04±0.01	0.04±0.01	0.04±0.01
Robustic acid	0.05±0.02	0.06±0.01	0.05±0.01	0.06±0.01
Lys-Thr-Gly	0.45±0.06	0.45±0.04	0.45±0.04	0.46±0.06
17beta-Nitro-5alpha-androstane	0.02±0.01	0.015±0.01	0.018±0.01	0.02±0.01
Nostoxanthin	0.016±0.01	0.017±0.01	0.018±0.01	0.02±0.01
7',8'-Dihydro-8'-hydroxycitraniaxanthin	0.012±0.01	0.013±0.01	0.015±0.01	0.018±0.01

$Pro_{/24h}$: 24-hours proteinuria; eGFR: estimated Glomerular Filtration Rate. No data achieved statistical significance.

http://dx.doi.org/10.21037/atm-20-2506

Table S7 Correlation between the Oxford classification of immunoglobulin A nephropathy and the top 10 fecal and serum metabolites

Bacteria	The Oxford Classification of IgA nephropathy							
	M0 (n=8)	M1 (n=7)	S0 (n=7)	S1 (n=8)	E0 (n=7)	E1 (n=8)	T0 (n=8)	>T0 (n=7)
Streptococcus	3440±1931	2843±1413	1524±526.1	2104±1821	2859±1572	2847±2559	2802±1581	3037±2471
Bacteroides	1793±717.5	3393±937.9	1435±1127	2416±767	1207±577.6	1834±231.2	1570±729.4	3601±806.9
Enterococcus	61.71±25.14	43.7±12.77	83.25±42.3	57.65±25.1	46.25±16.3	34.32±19.54	53.45±13.67	27.33±13.78
Fecal metabolite								
Gamma-L-Glutamyl-L -pipecolic acid	47.25±19.9	165.3±145.4	75.4±29.66	104.2±64.45	104.7±64.53	65.55±35.4	44.76±18.47	200.4±137.7
(2S,2'S)-Pyrosaccharopine	3.86±1.21	6.32±5.13	4.85± 0.96	5.0±2.41	5.68±2.27	3.6±2.05	3.69±1.12	8.08±4.92
11beta-PGF2alpha	0.37±0.27	0.36±0.25	0.24±0.11	0.24±0.11	0.45±0.24	0.09±0.02	0.44±0.25	0.11±0.03
PGG2	0.23±0.11	0.41±0.35	0.28±0.17	0.25±0.16	0.22±0.1	0.4±0.35	0.21±0.1	0.42±0.34
Cyclohexanecarboxylate	0.31±0.16	0.44±0.42	0.13±0.06	0.41±0.22	0.44±0.22	0.08±0.05	0.44±0.22	0.08±0.05
5-HETE	0.22±0.08	0.06±0.02	0.4374±0.2	0.10±0.03**	0.18±0.07	0.1±0.06	0.18±0.07	0.1±0.06
Verazine	0.08±0.04	0.02±0.01	0.08±0.07	0.04±0.02	0.08±0.04	0.01±0.01	0.07±0.04	0.03±0.01
Piperettine	0.02±0.01	0.02±0.01	0.02±0.02	0.02±0.01	0.02±0.01	0.02±0.01	0.02±0.01	0.02±0.01
5-HETrE	0.09±0.05	0.09±0.03	0.19±0.1	0.04±0.02*	0.1± 0.05	0.05±0.02	0.09±0.05	0.07±0.02
Capsaicin	0.15±0.12	0.08±0.04	0.2±0.19	0.07±0.02	0.15±0.1	0.07±0.05	0.14±0.11	0.08±0.04
Serum metabolite								
Leu-Leu-Phe	2.87±0.25	1.95±0.1	2.39±0.36	2.83±0.31	2.77±0.28	2.72±0.68	2.77±0.28	2.72±0.68
Brosimacutin A	0.08±0.03	0.18±0.01*	0.14±0.03	0.17±0.02	0.17±0.01	0.14±0.04	0.18±0.01	0.14±0.04
Docosahexaenoyl Serotonin	0.08±0.01	0.06±0.01	0.07±0.01	0.08±0.01	0.08±0.01	0.08± 0.02	0.08±0.01	0.08±0.02
Cadiamine	3.96±0.31	2.82±0.13	3.36±0.4	4.0±0.43	3.78±0.31	3.89±0.95	3.78±0.31	3.89±0.95
Lys-Cys-Ala	0.04±0.01	0.05±0.01	0.04±0.01	0.04±0.01	0.05±0.01	0.04±0.01	0.05±0.03	0.04±0.01
Robustic acid	0.03±0.02	0.06±0.01*	0.05±0.01	0.06±0.01	0.06±0.01	0.05± 0.02	0.06±0.01	0.05±0.02
Lys-Thr-Gly	0.37±0.01	0.48±0.03	0.44±0.05	0.47±0.05	0.47±0.04	0.46±0.1	0.47±0.04	0.46±0.1

E, endocapillary proliferation; M, mesangial hypercellularity; S, segmental sclerosis; T, tubular atrophy and interstitial fibrosis. *, P<0.05; **, P<0.01.

http://dx.doi.org/10.21037/atm-20-2506